

## Comparison of the Nanoparticles Performance in the Photocatalytic Degradation of a Styrene–Butadiene Rubber Nanocomposite

Tatiane M. Arantes,<sup>1</sup> Renata L. Sala,<sup>1</sup> Edson R. Leite,<sup>1</sup> Elson Longo,<sup>2</sup> Emerson R. Camargo<sup>1</sup>

<sup>1</sup>Department of Chemistry, LIEC—Interdisciplinary Laboratory of Electrochemistry and Ceramics, UFSCar—Federal University of São Carlos, CP 676, São Carlos 13565-905, SP, Brazil

<sup>2</sup>Department of Biochemistry and Technological Chemistry, LIEC-IQ, Chemistry Institute of Araraquara, UNESP—São Paulo State University, Rua Francisco Degni, CP 355, Araraquara 14801-907, SP, Brazil

Correspondence to: E. R. Camargo (E-mail: camargo@ufscar.br)

**ABSTRACT:** Much has been talking about the advantages of polymeric nanocomposites, but little is known about the influence of nanoparticles on the stability of these materials. In this sense, we studied the influence of both oxides of zirconium and titanium, known to have photocatalytic properties, as well as the influence of synthetic clay Laponite on the photodegradation of styrene–butadiene rubber (SBR). SBR nanocomposites were prepared by the colloidal route by mixing commercial polymer lattices and nanometric anatase TiO<sub>2</sub>, monoclinic ZrO<sub>2</sub> or exfoliated Laponite clays colloidal suspensions. To better understand the degradation mechanisms that occur in these nanocomposites, the efficiency of different photocatalysts under ultraviolet radiation was monitored by FT-IR and UV–vis spectroscopies and by differential scanning calorimetric. It was observed that TiO<sub>2</sub> and ZrO<sub>2</sub> nanoparticles undoubtedly acted as catalysts during the photodegradation process with different efficiencies and rates. However, when compared to pure SBR samples, the polymer degradation mechanism was unaffected. Unlike studies with nanocomposites montmorillonite, exfoliated laponite clay effectively acts as a photostabilizer of polymer UV photodegradation. © 2012 Wiley Periodicals, Inc. *J. Appl. Polym. Sci.* 128: 2368–2374, 2013

**KEYWORDS:** degradation; nanocomposites; colloids; rubber; nanoparticles; nanowires; nanocrystals

Received 30 January 2012; accepted 1 July 2012; published online 22 July 2012

**DOI:** 10.1002/app.38281

### INTRODUCTION

To overcome the limited performance of polymers, a new class of hybrid materials has emerged by the controlled insertion of nanoparticles into polymers. At the same time, numerous efforts have been expended searching for new materials focusing on higher performance with lower costs, greater durability and especially lower environmental impact. In this regard, polymer nanocomposites became the focus of many research groups because of their superior mechanical and thermal properties as compared to pure polymers and traditional composites.<sup>1–4</sup>

Many nanocomposite properties are dependent on the compatibility between nanoparticles and polymer chains and also on the dispersion of the particles in the matrix. There are several ways to insert nanoparticles in a polymeric matrix, including *in situ* polymerization, melting routes, mechanical extrusion and solution processing, but some of these routes in particular lead to intermediate colloidal dispersions of polymer macromolecules and nanoparticles. Colloidal mixtures have some advantages over other methods of synthesis due to their flexibility,

homogeneity at molecular level and simple experimental apparatus.<sup>3,5</sup> Although some nanoparticles can also act as catalysts in the polymer photodegradation process, there are only a few reports on degradation mechanisms in nanocomposites. However, what is quite clear is that the addition of some nanoparticles, especially titanium dioxide, can effectively photodegrade polymers by the generation of several active oxygen species when exposed to sunlight.<sup>4,6,7</sup>

On the other hand, styrene–butadiene rubber (SBR) is a well-known commercial elastomeric polymer used in the production of a wide range of products involving sectors that encompass new materials with superior characteristics. To better understand the degradation mechanisms that occur in polymer nanocomposites, we compared the efficiency of different nanoparticles under UV irradiation, some of them with known catalytic action in the photodegradation of polymers. These nanocomposites were prepared by the insertion of exfoliated laponite clay and synthetic TiO<sub>2</sub> and ZrO<sub>2</sub> nanoparticles with controlled size, shape and narrow size distributions through a colloidal route of synthesis. The effects of UV treatment on the photodegradation

behavior and rates were evaluated by means of infrared absorption spectroscopy (FTIR) and differential scanning calorimetry (DSC).

## EXPERIMENTAL

The solutions were prepared with deionized water obtained from a commercial Millipore Elix 3 system. All chemicals used in this work were analytical grade and were employed as received with no further purification.

### Synthesis of the Titanium Oxide Nanoparticles

Anatase TiO<sub>2</sub> nanoparticles were prepared by the method originally described by O'Brien et al.<sup>8</sup> by the dissolution of 0.185 mL of titanium (IV) isopropoxide (9%, Merck) under inert atmosphere to prevent premature hydrolysis in 30 mL of diphenyl ether (99.0 %, Merck) in the presence of oleic acid (99.0%, Merck), resulting in a solution with a nominal titanium concentration of 0.02 mol L<sup>-1</sup>. An aqueous solution of hydrogen peroxide (30%, Synth) was injected into the system (H<sub>2</sub>O<sub>2</sub>:Ti = 8 : 1) at 70°C under stirring to promote the controlled hydrolysis of the titanium alkoxide. The flasks were kept at 120°C for 12 h, after that the nanoparticles were isolated by centrifugation, washed with hexane, and dried.

### Synthesis of the Zirconium Oxide Nanoparticles

Stable colloids of monoclinic ZrO<sub>2</sub> nanoparticles were synthesized by hydrothermal processing of a 0.25 mol L<sup>-1</sup> solution prepared by the addition of 1.15 g of zirconium oxynitrate (99.5%, Aldrich) in 20 mL of deionized water. Hydrogen peroxide (30%, Synth) was rapidly added in the solution under vigorous stirring (H<sub>2</sub>O<sub>2</sub> : Zr = 8 : 1).<sup>9</sup> After mixing, the solution was placed in closed flasks and transferred to a stove. Hydrothermal treatments were performed at 110°C for 24 h and the stable colloids were dried in Petri dishes at 50°C for 30 min.

### Preparation of Nanocomposites

Aqueous colloidal suspensions of anatase TiO<sub>2</sub> nanoparticles (0.2% in mass), monoclinic ZrO<sub>2</sub> (1.0%) and exfoliated laponite clay (1.0 %) were prepared with the addition of 0.1 mol L<sup>-1</sup> of dodecylbenzenesulfonic acid (DBSA) as a surfactant in the dispersions of TiO<sub>2</sub> and ZrO<sub>2</sub>. Laponite clay aqueous dispersions were obtained by stirring vigorously the system for 1 h at room temperature. These aqueous colloidal dispersions of nanoparticles were added to SBR lattice and gently homogenized for 1 h. The colloidal dispersion of SBR nanocomposites with nanoparticles was then dried in Petri dishes in an air circulation oven at 50°C for several hours and then deployed as self-sustained nanocomposite films.

### Characterization

The nanoparticles were characterized by powder X-ray diffraction (XRD) using a Rigaku DMax 2500PC diffractometer with Cu K $\alpha$  radiation. The XRD patterns were collected at room temperature in the 2 $\theta$  range from 10 to 110° with a scan step of 0.02° and a step time of 1 s. Images of nanoparticles were obtained with a Carl Zeiss Supra 35VP high-resolution field-emission gun coupled to a scanning/transmission electron microscope. Samples were prepared for transmission electron microscopy (TEM) by dropping diluted nanoparticles dispersions on copper grids covered with a thin amorphous carbon

film. The absorption spectra in the UV-visible region (UV-vis) were collected using a Varian Cary 500, in the range 200–800 nm with scan rate of 1 nm s<sup>-1</sup>. The nanocomposites were analyzed by infrared absorption spectroscopy with a Fourier transform infrared spectrometer (Bruker Equinox 55) with an attenuated total reflectance accessory (ZnSe monocrystal). The spectra were collected at room temperature in the range 650–4000 cm<sup>-1</sup> with 32 scans and 4 cm<sup>-1</sup> of resolution. Samples were store for several weeks aiming to find the equilibrium with environmental humidity before the DSC measurements, which were taken with a Netzsch Phoenix 204 calorimeter in the range from 100 to 200°C at a heating rate of 20°C min<sup>-1</sup>.

### Photodegradation

Square samples with an area of 2 cm<sup>2</sup> and a thickness of 0.5 mm were prepared from the nanocomposites films containing the nanoparticles. These samples and the control film (without nanoparticles) were placed in a dark box and set at distance of 10 cm from the UV source to perform the photodegradation reactions. The radiation used in this experiment was obtained with a medium-pressure mercury vapor lamp (Osram, HQL 400) without the protection bulb.

## RESULTS AND DISCUSSION

All the peaks observed in the X-ray pattern of TiO<sub>2</sub> in Figure 1(a) were attributed to the anatase phase in accordance with the powder diffraction file (PDF) 21-1272. These nanoparticles were obtained by the controlled hydrolysis of titanium (IV) isopropoxide with hydrogen peroxide diluted in diphenyl ether and oleic acid acting as the surfactant. Some peaks from the aluminum sample holder could be identified and are indicated in the pattern. The morphology of anatase nanoparticles was characterized by transmission electron microscopy (TEM) and the image shows nanoparticles with diameters of ~5 nm [Figure 1(b)]. Pure ZrO<sub>2</sub> nanoparticles were obtained by the hydrothermal processing of zirconium oxynitrates in the presence of hydrogen peroxide. The XRD pattern in Figure 1(d) shows a monoclinic ZrO<sub>2</sub> phase in agreement with the PDF 37-1484. The TEM image of Figure 1(e) shows that this route of synthesis provides well dispersed nanocrystalline ZrO<sub>2</sub> in the range from 5 to 15 nm with an oriented attachment as the main growth mechanism. Figure 1(c, f) shows, respectively, the UV-vis spectra of TiO<sub>2</sub> and ZrO<sub>2</sub> nanoparticles. It was observed the characteristic absorption band with a band gap of 3.4 eV for TiO<sub>2</sub>; however two values were calculated for ZrO<sub>2</sub>. While the typical band gap of ZrO<sub>2</sub> was observed at 4.5 eV, the second value of 3.5 eV is related to an indirect band gap sometimes observed in nanometric particles.

On the other hand, Laponite is a commercial name of the synthetic clay produced and sold by Southern Clay Products (USA). It is a layered material that is easily dissolved in an aqueous medium, resulting in a transparent and water-soluble gel with a viscosity proportional to the amount of clay used.<sup>10</sup> The SBR used in this study was industrially produced in latex form, which can be described as an aqueous colloidal dispersion of polymeric spherical particles with a diameter of ~0.5  $\mu$ m.

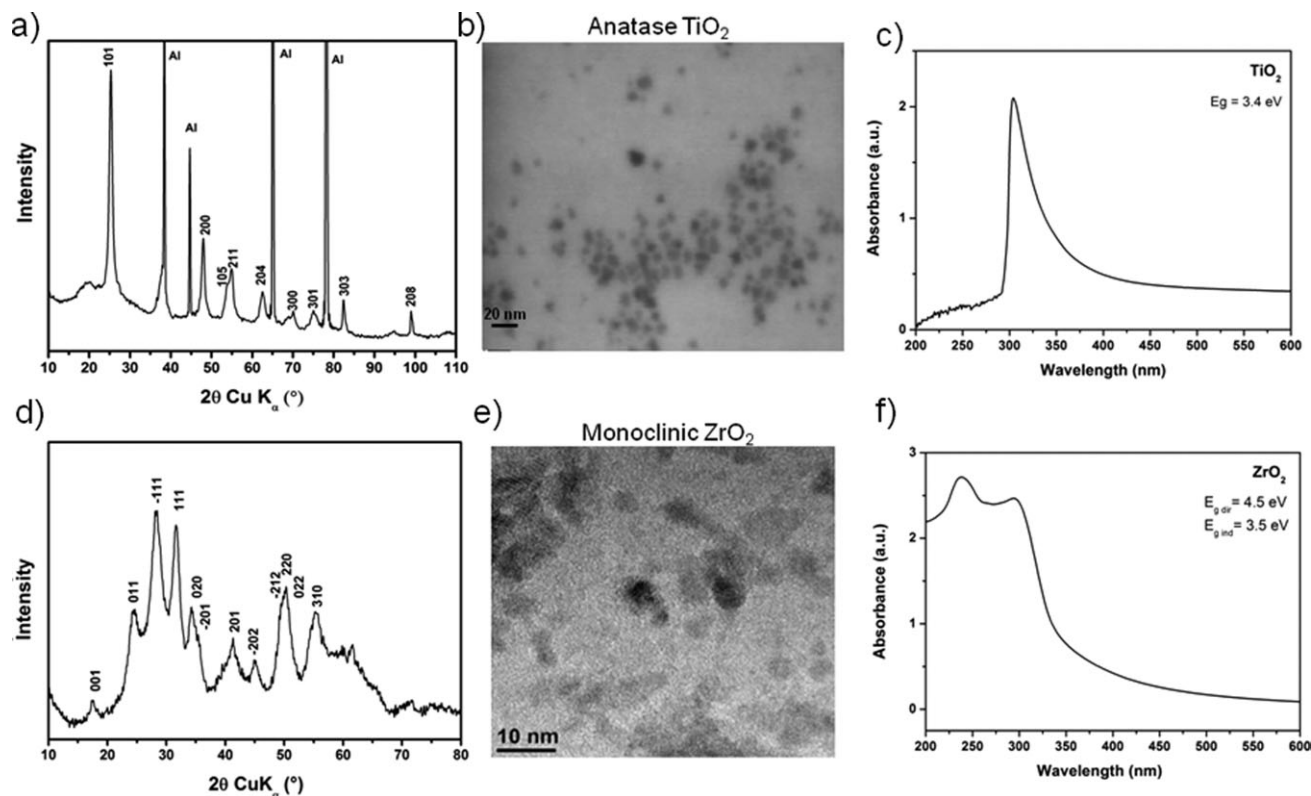


**Figure 1.** (a) XRD pattern of anatase  $\text{TiO}_2$ , (b) TEM image of  $\text{TiO}_2$  nanoparticles, (c) UV-visible spectroscopy of  $\text{TiO}_2$  nanoparticles, (d) XRD pattern of monoclinic  $\text{ZrO}_2$  nanoparticles, (e) TEM micrograph of  $\text{ZrO}_2$  nanoparticles, (f) UV-vis spectrum  $\text{ZrO}_2$  nanoparticles. Al indicates the aluminum substrate.

When the soluble laponite gel is added to the polymer latex under mechanical homogenization, a complex and stable colloidal system is obtained. Valadares et al.<sup>5</sup> found evidences of a strong compatibility between montmorillonite lamellae and the surface of natural rubber colloids. By transmission electron microscopy, they observed some lamellae curved and adhered on the surface of the polymer colloidal particles due to the presence of counter ions clustered between them. The existence of this interaction is the key point to obtain uniform nanocomposites from a dispersion of inorganic nanoparticles and polymeric macromolecules through solvent elimination.<sup>11,12</sup>

In this study, nanocomposites of SBR and different nanoparticles (Laponite, anatase  $\text{TiO}_2$  and monoclinic  $\text{ZrO}_2$ ) were prepared at room temperature by a method that offers the advantage of combining the flexibility of processing single mixtures of high homogeneity with aspects of green chemistry. Colloidal dispersions of hydrophilic  $\text{TiO}_2$  or  $\text{ZrO}_2$  nanoparticles with the surface modified with DBSA were added to the commercial aqueous colloidal dispersions of SBR. Self-sustained and highly homogeneous films were easily prepared by removing the solvent. During this stage, SBR colloids agglutinated and the nanoparticles were trapped, resulting in SBR nanocomposites films containing 0.2% of  $\text{TiO}_2$  nanoparticles and 1.0%  $\text{ZrO}_2$  nanoparticles, respectively. It is well known that  $\text{TiO}_2$  is a much more efficient photocatalyst than  $\text{ZrO}_2$ . For this reason, to adjust the photodegradation rate to the same time scale, it was necessary to use a larger amount of  $\text{ZrO}_2$  nanoparticles to obtain a similar

effect on the polymeric degradation observed with  $\text{TiO}_2$ . Nanocomposites of SBR with 1.0% in mass of laponite were prepared by the same route but without the use of any surfactant.

In our previous work, we studied the effect of titanium dioxide nanoparticles in the mechanism of polymer photodegradation.<sup>11,12</sup> Thus, we are now studying the influence of different nanoparticles on the photodegradation of the SBR nanocomposite matrix. All nanocomposites and pure SBR films were exposed to UV light for different time intervals up to 96 h, and their attenuated total reflectance infrared spectra are shown in Figure 2. It is known that titanium dioxide is an efficient photocatalyst capable of generating reactive oxygen species that degrade the polymer.<sup>11,13–15</sup> When semiconductor oxides such as  $\text{TiO}_2$  or  $\text{ZrO}_2$  are irradiated with photons of energy equal to or greater than its energy gap, electrons in the conduction band can generate holes or vacancies in the valence band that are responsible by the oxidation reaction.<sup>16–18</sup> Photocatalytic degradation of polymers is triggered by active oxygen species such as  $\cdot\text{O}_2^-$ ,  $\cdot\text{HOO}$  and  $\cdot\text{HO}$ , which are formed on the surface of the catalyst nanoparticles. These active oxygen species attack the polymer chain, removing hydrogen and forming radical carbon successively until the polymer chain be cleaved.<sup>6,11,14</sup>

There are several studies about the photo-oxidative degradation of polymers containing polybutadiene groups, such as butadiene rubber (BR), styrene-butadiene rubber SBR,<sup>19,20</sup> nitrile rubber (NBR)<sup>21</sup> and acrylonitrile-butadiene-styrene (ABS).<sup>22,23</sup> Usually,

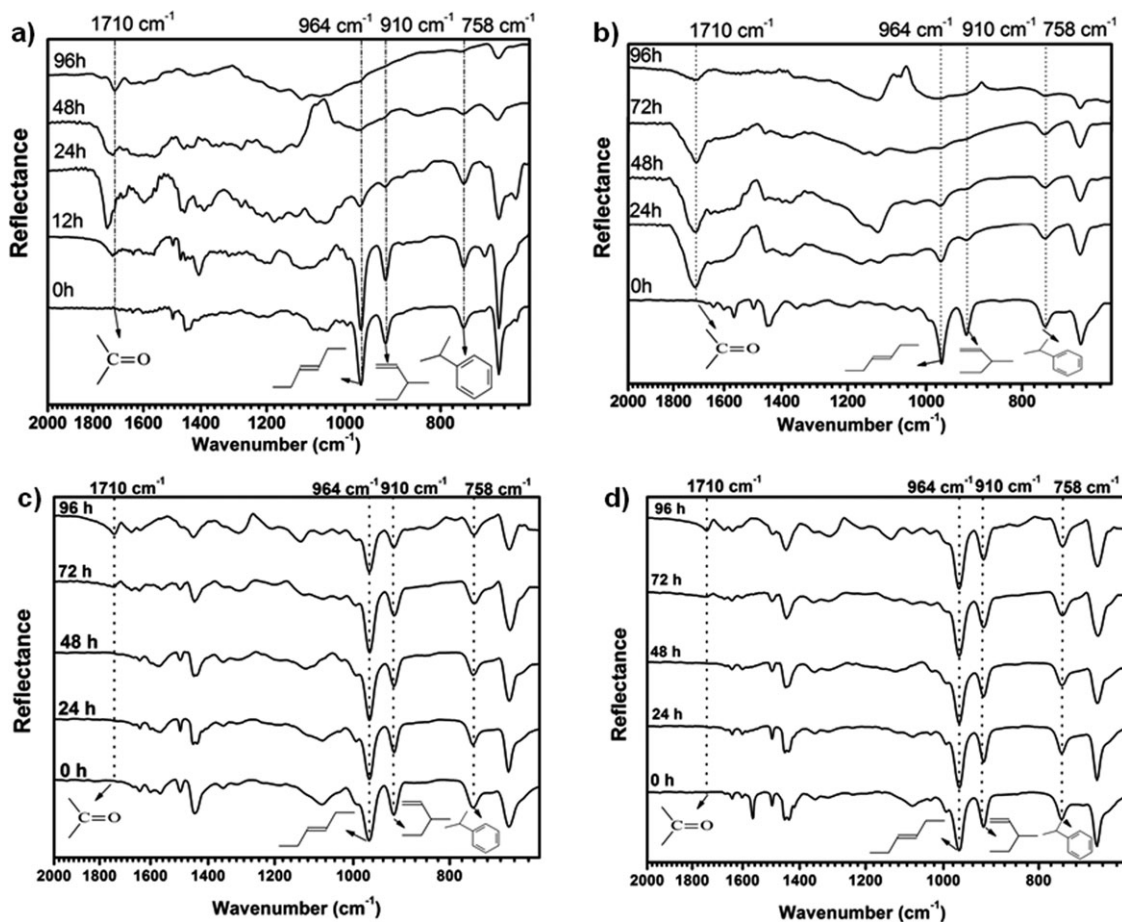


**Figure 2.** FTIR SBR nanocomposites illuminated with a mercury lamp of 400 W for different photodegradation times: (a) SBR and TiO<sub>2</sub> (0.2%), (b) SBR and ZrO<sub>2</sub> (1.0%), (c) SBR and Laponite (1.0%), (d) pure SBR.

these studies are based on the exposure of the polymers to ultraviolet radiation. It has been suggested that polymer degradation is mainly controlled by the reactivity of 1,2-butadiene and of *cis*- and *trans*-1,4-butadiene isomers. These isomers appear to be degraded by similar mechanisms, but the 1,2-butadiene seems to form radical species more readily than 1,4-butadiene isomers because of the existence of labile hydrogen in tertiary carbons. The degradation begins with a photon that catalyzes the formation of a peroxide alkyl radical through the elimination of the labile hydrogen. This radical recombines with double bonds of butadiene groups and forms an epoxy radical that propagates the degradation to other double bonds. Instead of forming an epoxy intermediate, sometimes the peroxide radical captures hydrogen to produce an alkyl hydroperoxide radical. This radical propagates the degradation through the formation of carbonyl groups in several ways, decreasing the amount of double bonds. Adam et al.<sup>20,21</sup> conducted comparative studies about the photodegradation of NBR and SBR, and similarities in their mechanism of photodegradation were found. They observed that the hydroperoxides initially formed, mainly in allylic units of butadiene, are broken down into alcohols and the  $\alpha$ ,  $\beta$ -unsaturated ketones are photo-oxidized to saturated acids. At the same time, photons absorbed by the aromatic rings are transferred to the tertiary carbon located

near this group, forming hydroperoxide radicals that propagate the degradation through  $\alpha$ , $\beta$ -unsaturated carbonyl groups, preserving the aromatic ring.

Figure 2 shows that the vibrational modes associated with *trans*-1,4-butadiene (at 964 cm<sup>-1</sup>) and 1,2-butadiene (at 910 cm<sup>-1</sup>) groups diminished in all nanocomposites and pure SBR, whereas the carbonyl band (at 1710 cm<sup>-1</sup>) increased simultaneously, but at different rate. These results suggest that double bonds of butadiene groups were rapidly oxidized by the species generated on TiO<sub>2</sub> and ZrO<sub>2</sub> nanoparticles. Obviously, benzene rings can also absorb UV light and gradually form radicals. However, the aromatic band at 758 cm<sup>-1</sup> of the nanocomposites with TiO<sub>2</sub> [Figure 2(a)] was unaffected up to 48 h of exposure to UV radiation and to 72 h for the nanocomposites with ZrO<sub>2</sub> [Figure 2(b)]. On the other hand, butadiene bands (at 964 and 910 cm<sup>-1</sup>) decreased their intensities under exposure to UV radiation after 12 h [Figure 2(a)], indicating a selective kinetic attack of the oxidizing agent on the double bond. In the case of laponite nanocomposites [Figure 2(c)] and pure SBR [Figure 2(d)], all spectra are quite similar even after the exposure to UV radiation up to 96 h, showing that the nanocomposites with TiO<sub>2</sub> and ZrO<sub>2</sub> are photodegraded faster than the nanocomposites with laponite.

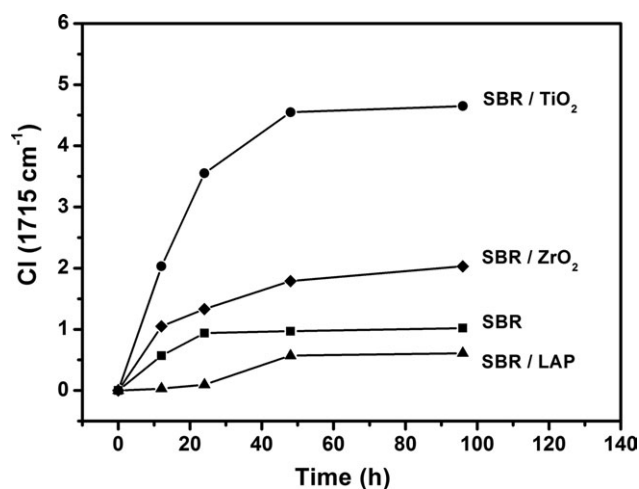


**Figure 3.** Carbonyl index (CI) for different photodegradation times of the SBR and TiO<sub>2</sub> (0.2%) nanocomposite (SBR/TiO<sub>2</sub>), SBR and ZrO<sub>2</sub> (1.0%) nanocomposite (SBR/ZrO<sub>2</sub>), pristine rubber (SBR), and SBR and Laponite (1.0%) nanocomposite (SBR/LAP).

Previous studies about thermal and photochemical degradation of nanocomposites reported photocatalytic effects associated with exfoliate clays during the photodegradation of different polymeric matrices,<sup>24–29</sup> but only a few works focused on elastomeric compounds.<sup>21</sup> Although mechanical, thermal and rheological properties of clay/polymer nanocomposites are typically superior to traditional materials,<sup>1,2</sup> some pristine polymers show higher photoresistance to UV exposure due to their higher degree of crystallinity. Moreover, the decomposition of the ammonium ions usually present in organoclays forms new catalytic sites. The catalytic effect of impurities present in several clays and the migration of antioxidant agents onto the clay, which reduces its effect, can also accelerate the photodegradation process in nanocomposites.

Jubete et al.<sup>30</sup> used the ratio of the intensity of the carbonyl band (1715 cm<sup>-1</sup>) and the aromatic vibration (1492 cm<sup>-1</sup>) to evaluate the catalytic photodegradation efficiency [eq. (1)], which was referred to as the carbonyl index (CI). This number, which is proportional to the intensity of the carbonyl band relative to an internal reference, estimates the oxidation degree of the material and can be used to compare the photodegradation rate for each nanocomposite. The values (Abs<sub>1715</sub><sup>\*</sup>) and (Abs<sub>1492</sub><sup>\*</sup>) in eq. (1) are the initial absorbance and (Abs<sub>1715</sub>) and (Abs<sub>1492</sub>) are the values after the photodegradation.

$$CI = \frac{Abs_{1715}}{Abs_{1492}} - \frac{Abs_{1715}^*}{Abs_{1492}^*} \quad (1)$$

The carbonyl index calculated after 96 h of UV exposure for nanocomposites with 0.2% of TiO<sub>2</sub> (CI = 4.65) was almost twice that calculated for nanocomposites with 1.0% of ZrO<sub>2</sub> nanoparticles (CI = 2.03) indicating that the photodegradation efficiency is directly related to the type of nanoparticles used. For comparison purposes, the carbonyl index of pure SBR was of 1.02 for the same condition. The CI values calculated as a function of UV exposure are shown in Figure 3. It is possible to

note that the carbonyl indices remain approximately constant after 48 h. It occurs because, initially, the 1,4 and 1,2-butadiene groups of SBR are oxidized to form unstable  $\alpha,\beta$ -unsaturated ketones carbonyl compounds. In sequence, these unstable groups quickly change to more stable carbonyl compounds, which keep the intensity ratio between (Abs<sub>1715</sub>) and (Abs<sub>1492</sub>) unchanged. It can also be observed that pristine polymers have a higher photodegradation rate than laponite SBR nanocomposites (SBR/LAP), which shows that, unlike studies with nanocomposites using montmorillonite, Laponite clay effectively acts as a photostabilizer of polymer UV photodegradation, since its presence retarded the photochemical process of degradation.<sup>31</sup>

During the photodegradation process, crosslinked bonds are formed between polymer chains, hardening the material and consequently increasing the glass-transition temperature ( $T_g$ ). These reactions occur particularly in the chains containing  $\alpha,\beta$ -unsaturated carbonyls, which make the material stiffer and less soluble in organic solvents. Figure 4 shows the DSC curves of the pure polymer and of nanocomposites after 300 h of UV exposure. The transition temperature in pure SBR (−49.3°C) is clearly observed as a modification in the base line and is characterized by a second-order transition. On the other hand, all degraded nanocomposites show the typical curve of vulcanized rubber without a visible transition temperature. The  $T_g$  of the nanocomposite with ZrO<sub>2</sub> (−40.9°C) is almost 9°C higher than the  $T_g$  calculated for pure polymers. For nanocomposites with TiO<sub>2</sub>, the transition temperature (−16.8°C) is almost 32°C higher, indicating that TiO<sub>2</sub> nanoparticles are more efficient in forming crosslinking bonds in the polymer than ZrO<sub>2</sub>. After 300 h of UV exposure, SBR/LAP nanocomposites and pristine SBR suffered only a small increase in the transition temperature (~2°C), which is in agreement with the lower photodegradation degree compared to TiO<sub>2</sub> and ZrO<sub>2</sub> nanocomposites (Figure 3). In our previous article,<sup>12</sup> pure SBR elastomer, SBR/TiO<sub>2</sub> nanocomposite, and SBR/TiO<sub>2</sub> photodegraded nanocomposite were analyzed by solid-state <sup>13</sup>C nuclear magnetic resonance (NMR). Solid-state <sup>13</sup>C NMR was used to characterize the structural and dynamic behavior, evaluating the domain molecular mobility of the pure elastomer and of the nanocomposites before and after photodegradation. Analyzing the pure SBR and the SBR/TiO<sub>2</sub> nanocomposites spectra according to variable contact-time (VCT) experiments, it was encountered two domains with very different relaxation times, which is intimately associated with molecular mobility, indicating a heterogeneous system. The signal distribution profile shows clearly a large and flexible domain for the pure SBR and SBR/TiO<sub>2</sub> nanocomposite samples, but a rigid domain for the SBR/TiO<sub>2</sub> photodegraded nanocomposite. These results confirm what was shown by DSC measurements.

In summary, from the results of photodegradation presented in Figures 2 and 3, it is possible to say that the same sequence of degradation reactions observed in pure SBR also occurs in the nanocomposites but at different rates, which supports the important conclusion that the degradation mechanism is not affected by the composition of the catalyst, although the degradation rate is dependent on the composition, shape and catalyst size, it was observed that the photodegradation mechanism is a

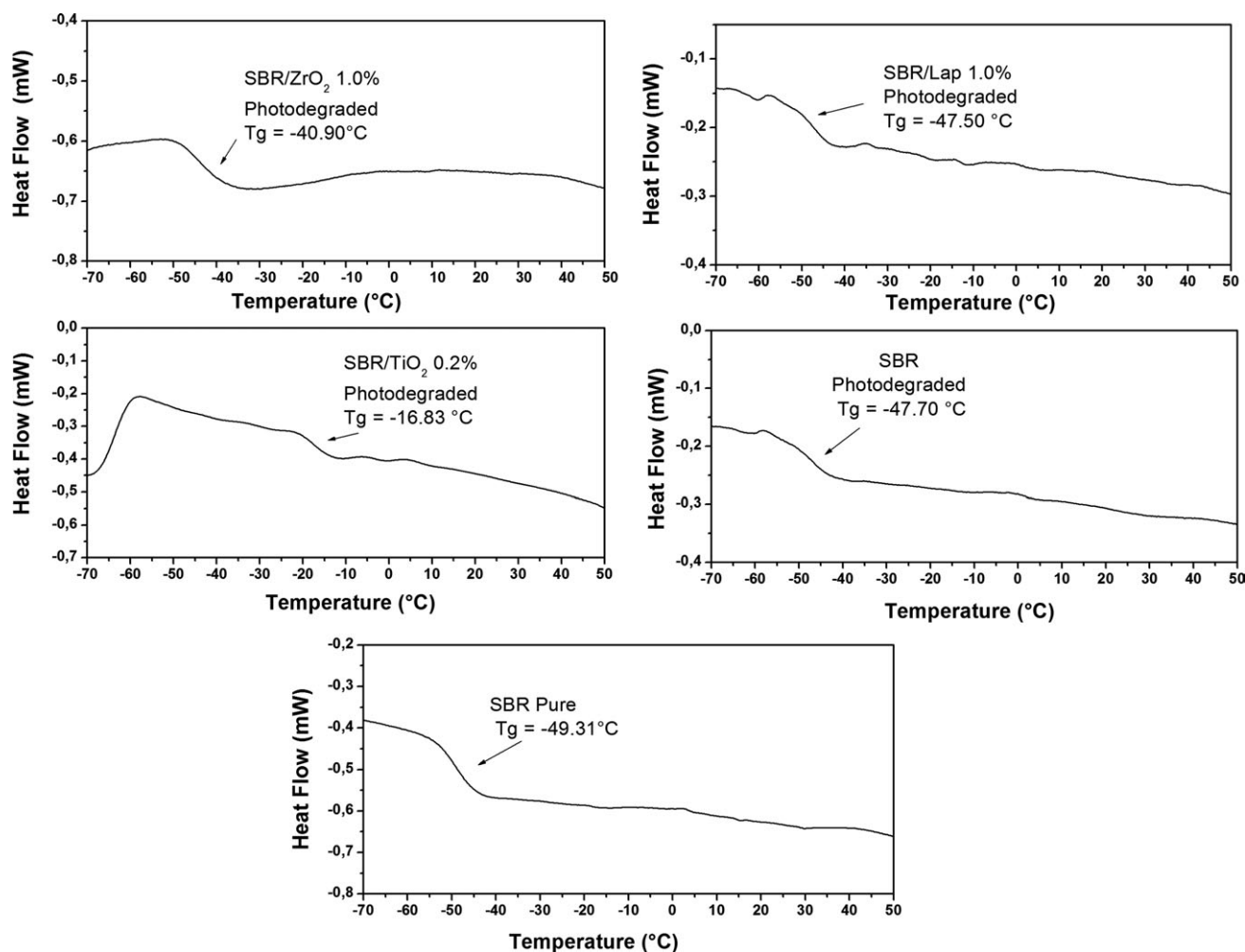


**Figure 4.** DSC curves for the pristine rubber (SBR) before exposition to UV radiation and (SBR deg) after 300 h of photodegradation. The DSC curves of SBR/TiO<sub>2</sub>, SBR/ZrO<sub>2</sub>, and SBR/Laponite nanocomposites were obtained from samples after 300 h of photodegradation.

characteristic of the polymer, which gives a key to new solutions to improve the technological applications of this class of materials. Several particles and nanoparticles have been widely used to obtain composite and nanocomposites for different applications and some of these nanoparticles can also photocatalyze the polymeric matrix. However, since the mechanism of polymer degradation is not affected by the chemical nature of nanoparticles, this undesired side effect can be controlled, or even vanished, applying traditional techniques already developed to protect pure polymers. This extra protection of the polymeric matrix can play an important role in sectors where the photodegradation could represent a drawback in the performance of devices based in nanocomposites, for instance in aerospace and medical industrial sectors.

## CONCLUSIONS

The colloidal route is a suitable method to prepare nanocomposites from polymers in latex form and synthetic nanoparticles or exfoliated clays. Nanoparticles of anatase TiO<sub>2</sub> and monoclinic ZrO<sub>2</sub>, which were used in the preparation of nanocomposites with SBR, undoubtedly acted as catalysts in the polymer matrix

photodegradation, but the mechanism of polymer degradation was unaffected by the nature of nanoparticles, although degradation rate showed strong dependence with nanoparticles properties and with the amount of nanoparticles inserted in the nanocomposite. Nanocomposites of SBR and 0.2% in mass of TiO<sub>2</sub> nanoparticles were degraded about two times faster than those with a 1.0% of ZrO<sub>2</sub> and about four times faster than pure polymer. On the other hand, exfoliated Laponite layers effectively acted as photostabilizer against UV photodegradation. These observations allowed us to reach an important conclusion: that the presence of different polymeric nanoparticles provides a matrix to obtain nanocomposites with different properties and stabilities, and their behavior before the photobleaching is strongly dependent on the composition of the nanoparticles. Namely, that actually affects the composition of nanoparticles in nanocomposites photostability, and is not an effect from of the organic–inorganic interface (polymer/nanoparticle).

## ACKNOWLEDGMENTS

The financial support from FAPESP (2007/50904-2 and 2007/58891-7), FINEP, CNPq (470009/2010-1) and CAPES is gratefully

acknowledged. The INCTMN/CMDMC also provided support for this work.

## REFERENCES

- Alexandre, M.; Dubois, P. *Mater. Sci. Eng.* **2000**, *28*, 1.
- Winey, K. I.; Vaia, R. A.; *MRS Bull.* **2007**, *32*, 314.
- Oberdisse, J. *Soft Matter.* **2006**, *2*, 29.
- Esteves, A. C. C.; Timmons, A. B.; Trindade, T.; *Quim. Nova* **2004**, *27*, 798.
- Valadares, L. F.; Leite, C. A. P.; Galembeck, F.; *Polymer* **2006**, *47*, 672.
- Zan, L.; Tian, L.; Liu, Z.; Peng, Z. *Appl. Catal. A* **2004**, *264*, 237.
- Mertz, G.; Hassouna, F.; Toniazzo, V.; Dahoun, A.; Ruch, D. *J. Eng. Mater. Technol.* **2012**, *13*, 010903.
- Ó'Brien, S.; Brus, L.; Murray, C. B. *J. Am. Chem. Soc.* **2001**, *123*, 12085.
- Arantes, T. M.; Mambriani, G. P.; Stroppa, D. G.; Leite, E. R.; Longo, E.; Ramirez, A. J.; Camargo, E. R. *J. Nanopart. Res.* **2010**, *12*, 3105.
- Nicolai, T.; Cocard, S. *Langmuir* **2000**, *16*, 8189.
- Arantes, T. M.; Leite, E. R.; Longo, E.; Camargo, E. R. *J. Appl. Polym. Sci.* **2009**, *113*, 1898.
- Arantes, T. M.; Leão, K. V.; Tavares, M. I. B.; Ferreira, A. G.; Longo, E.; Camargo, E. R. *Polym. Test.* **2009**, *28*, 490.
- Jiang, C.; Guo, Y.; Hu, C.; Wang, C.; Li, D. *Mater. Res. Bull.* **2004**, *39*, 251.
- Navio, J. A.; Hidalgo, M. C.; Colon, G.; Botta, S. G.; Litter, M. I. *Langmuir* **2001**, *1*, 202.
- Fa, W.; Yang, C.; Gong, C.; Peng, T.; Zan, L. *J. Appl. Polym. Sci.* **2010**, *118*, 378.
- Maia, D. R. J.; Balbinot, L.; Popi R. J.; De Paoli, M. A. *Polym. Degrad. Stab.* **2003**, *82*, 89.
- López-Salinas, E.; Hernández-Cortéz, J. G.; Cortés-Jácome, Ma. A.; Navarrete, J.; Ma, E.; Vázquez, A.; Armendáriz, H.; López, T. *Appl. Catal. A* **1998**, *175*, 43.
- Reddy, V. R.; Hwang, D. J.; Lee, S. *Korean J. Chem. Eng.* **2003**, *20*, 1026.
- Bousquet, J. A.; Fouassier, J. P. *Eur. Polym. J.* **1987**, *23*, 367.
- Adam, C.; Lacoste, J.; Lemaire, J. *Polym. Degrad. Stab.* **1989**, *26*, 269.
- Adam, C.; Lacoste, J.; Lemaire, J. *Polym. Degrad. Stab.* **1990**, *27*, 85.
- Piton, M.; Rivaton, A. *Polym. Degrad. Stab.* **1997**, *55*, 147.
- Adeniyi, J. B.; Kolawole, E. G. *Eur. Polym. J.* **1984**, *20*, 43.
- Lonkar, S. P.; Kumar, A. P.; Singh, R. P. *Polym. Adv. Technol.* **2007**, *18*, 891.
- Dintcheva, N. T.; Filippone, G.; La Mantia, F. P.; Acierno, D. *Polym. Degrad. Stab.* **2010**, *95*, 527.
- Morlat-Therias, S.; Mailhot, B.; Gardette, J. L.; Silva, C.; Haidar, B.; Vidal, A. *Chem. Mater.* **2005**, *17*, 1072.
- Mailhot, B.; Morlat, S.; Gardette, J. L.; Boucard, S.; Duchet, J.; Gérard, J. F. *Polym. Degrad. Stab.* **2003**, *82*, 163.
- Diagne, M.; Guèye, M.; Dasilva, A.; Vidal, L.; Tidjani, A. *J. Mater. Sci.* **2006**, *41*, 7005.
- Morlat, S.; Mailhot, B.; Gonzalez, D.; Gardette, J. L. *Chem. Mater.* **2004**, *16*, 377.
- Jubete, E.; Liauw, C. M.; Jacobson, K.; Allen, N. S. *Polym. Degrad. Stab.* **2007**, *92*, 1611.
- Ranby, B.; Rabek, J. F. *Photodegradation, Photo-oxidation and Photostabilization of Polymers*; Wiley: London, **1975**; Chapter 10, p 362.